Anomalous transport and metal to half-metal evolution induced by Cr doping in Co$_2$FeGa

Zezhong Li,[1] Jieqiong Cheng,[1] Qiangqiang Zhang,[1] Enke Liu,[2] and Zhuhong Liu [1,*]

[1]*Department of Physics, University of Science and Technology Beijing, Beijing 100083, China*
[2]*Beijing National Laboratory for Condensed Matter Physics, Institute of Physics,*
Chinese Academy of Sciences, Beijing 100190, China

This paper aims to enhance the spin polarization of the Heusler alloy Co$_2$FeGa by replacing Co with Cr. It is found that, as the substitution content x increases from $0 \rightarrow 1 \rightarrow 2$ in Co$_{2-x}$Cr$_x$FeGa alloys, the Fermi level in the spin-up direction is tuned from the low density of states (DOS) of hybridized orbital t_{2g} to the small pseudogap between e_g and t_{1u} and finally to the area of high DOS formed by the antibonding t_{1u} and e_u hybridized orbitals. Meanwhile, the Fermi level of the spin-down direction remains in the pseudogap. Hence a transition from a ferromagnetic metal ($x = 0$) to a ferrimagnetic (FIM) spin-gapless semiconductor (SGS; $x = 1$) and further to a FIM near half-metal (HM) ($x = 2$) was realized with the spin polarization enhanced from 63% to 95%. Furthermore, the disorder between Cr(B) and Ga does not destroy the HM property of Cr$_2$FeGa. Theoretically, the intrinsic anomalous Hall conductivity induced by the Berry curvature is found to increase with doping Cr in ordered Co$_{2-x}$Cr$_x$FeGa. Experimentally, the saturation magnetic moments of Co$_2$FeGa and CoCrFeGa were measured to be 5.21 μ_B/f.u. and 2.25 μ_B/f.u. at 5 K, respectively, which is consistent with first-principles calculations. However, in Cr$_2$FeGa, there is an obvious deviation between the experimental value of 0.36 μ_B/f.u. at 5 K and the calculated value of 0.96 μ_B/f.u., which is attributed to the swap disorder in the sample. The longitudinal resistivity shows Co$_2$FeGa a metallic conductor behavior, whereas both CoCrFeGa and Cr$_2$FeGa exhibit semiconductorlike behavior from 5 to 350 K. In the compound CoCrFeGa, the small anomalous Hall conductivity (σ_{xy}^A) of 52.7 S/cm at 5 K is in line with the property of SGS. Both intrinsic and extrinsic factors contribute to the anomalous Hall effect in CoCrFeGa, with the intrinsic contribution being larger than that of the extrinsic part. For Cr$_2$FeGa, a maximum of the value of σ_{xy}^A 14.1 S/cm is observed at 5 K, and this value goes to zero above 150 K due to Curie transition.

I. INTRODUCTION

Half-metal (HM) was first proposed in 1983 by de Groot *et al.* when they employed *ab initio* calculations to investigate the properties of the half-Heusler alloy NiMnSb [1]. HM holds 100% spin polarization, with semiconducting behavior for one spin direction but the metallic behavior for the other. HM has been highly considered due to its use in high tunnel magnetoresistance devices and spintronic devices [2,3] utilizing spin as a carrier of information. Furthermore, it has been found that certain half-metallic materials exhibit nontrivial topological structures, such as Weyl points and nodal line. These unique topological features generate a large Berry curvature, resulting in the observation of a giant anomalous Hall effect (AHE) in these half-metallic materials, i.e., Co$_2$MnGa [4], Co$_2$MnAl [5] and Co$_3$Sn$_2$S$_2$ [6]. The remarkable magnetotransport properties of these materials further promote the application prospects of HM in the field of spintronics devices, offering reduced energy costs.

Compared with many half-metallic materials, such as metal oxides, perovskites, and double perovskites [7,8], Co-based Heusler alloys are more suitable for application because of their high Curie temperature (T_C) [9,10] and variable

properties acquired by tuning valence electron counts [11–13]. As a unique variant of HM, spin-gapless semiconductors (SGSs) also possess full spin polarization and features a finite band gap for one spin direction, while behaving as a semimetal for the other spin direction due to the touching of conduction and valence band edges [14].

Heusler alloys are intermetallic compounds whose formula is X_2YZ, where X and Y are transition metal elements and Z is a main group element. Conventional full Heusler compounds crystallize in a cubic crystal system (space group $Fm\bar{3}m$, #225) named $L2_1$ phase, and the atoms X, X, Y, and Z in the unit cell occupy the positions with Wyckoff coordinates: A $(0, 0, 0)$, C $(1/2, 1/2, 1/2)$, B $(1/4, 1/4, 1/4)$, and D $(3/4, 3/4, 3/4)$ along the body diagonal. However, when the number of valence electrons of the Y element exceeds that of the X element, X, X, Y, and Z will occupy sites A, B, C, and D successively, resulting in an XA phase structure known as an inverse Heusler alloy. This structure belongs to space group $F\bar{4}3m$ (#216). Furthermore, when one X is substituted with a distinct transition metal element X' forming $XX'YZ$, a Y-type quaternary Heusler alloy with the identical space group $F\bar{4}3m$ is formed.

Although quite a few Co-based and Mn-based Heusler alloys have been predicted to be HM, it is important to note that there are still many stoichiometric Heusler alloys that do not possess this property. However, by appropriately

---

*Corresponding author: zhliu@ustb.edu.cn

224407-1

adjusting the valence electron count, these alloys can be transformed into half-metallic materials. For example, in the alloy $Co_2MnAs_xAl_{1-x}$, when x is between 0.5 and 0.75, the Fermi level (E_F) falls within the gap of the spin-down channel, forming a perfect HM [15]. In the alloy $Co_2MnAl_xSi_{1-x}$, it is demonstrated that the E_F shifts toward the center of the half-metallic gap with x, realizing a more strong half-metallicity property [16]. The doped compound $Co_2FeAl_{0.5}Si_{0.5}$ hosts strong half-metallicity whereas the corresponding stoichiometric composition does not [17]. A double element doping in CoFeCrGe can achieve the strong half-metallicity in the compound $CoFeCr_{0.75}V_{0.25}Ge_{0.5}As_{0.5}$ [18]. In the alloy $Co_{2-x}Cr_xFeGe$, the Cr substitution moves the E_F toward the center of the half-metallic gap while also increasing the majority spin density of states (DOS) at E_F [19].

Ferromagnetic Co_2FeGa has a high T_C of approximately 1100 K [20], but it is not a complete HM. It has been found that Co_2FeGa can be modulated into a half-metallic material through doping. Ahmadian and Boochani have indicated that the Ti doping compound $Co_2Fe_{1-x}Ti_xGa$ turns into a perfect HM when $x = 0.5$ [21]. In the Ge doping partial Ga alloy $Co_2FeGa_{1-x}Ge_x$, the complete half-metallicity is achieved in theoretical calculation, and a high experimental spin polarization value of 69% is obtained when $x = 0.5$ [22]. These methods try to transform the spin-down pseudogap around E_F into a genuine gap, ultimately achieving half-metallicity. However, instead of tailoring the spin-down pseudogap, we concentrate on the low DOS at E_F in the spin-up direction and aim to enhance the spin polarization by reducing the number of valence electrons, thus adjusting the E_F to a higher DOS range. In this study, we adopt the approach of replacing the Co atom with a Cr atom to achieve this tuning. It turns out that a transition from a ferromagnetic (FM) metal to a near ferrimagnetic (FIM) SGS and further to a near FIM half-metal has been realized in $Co_{2-x}Cr_xFeGa$ ($x = 0$, 1, and 2) alloys. The electronic, magnetic, and transport properties of the three alloys have been extensively investigated by combining first-principles calculations with experimental research.

II. EXPERIMENTAL AND COMPUTATIONAL DETAILS

Polycrystalline ingots with nominal compositions of $Co_{2-x}Cr_xFeGa$ ($x = 0$, 1, and 2) were synthesized by arc melting Co, Fe, Cr, and Ga with a purity of 99.99% in a highly purified argon atmosphere. To achieve chemical homogeneity, each ingot was remelted four times and flipped before a new melting step. All the ingots were sealed in a quartz tube under argon atmosphere and then annealed at 1073 K for 3 days, followed by naturally cooling down to room temperature. The crystal structure was identified by standard x-ray diffraction (XRD) using a Rigaku Smartlab3 instrument with Cu $K\alpha$ radiation. The longitudinal and Hall resistivities were measured simultaneously using a six-probe method on the same bar-shape sample with a Quantum Design physical properties measurement aystem (PPMS). The magnetic properties were also measured in the PPMS device.

We have employed the Vienna *ab initio* simulation package (VASP) [23] in our calculations within density functional theory to investigate the electronic properties of $Co_{2-x}Cr_xFeGa$ ($x = 0$, 1, and 2). The generalized gradient approximation

in the scheme of Perdew-Burke-Ernzerhof [24] are adopted for the electronic exchange-correlation functional. The plane-wave cutoff energy of 500 eV and the self-consistent field convergence criterion of 10^{-7} eV/cell for energy are set in the calculations. The $15 \times 15 \times 15$ k-point setting was adopted for Brillouin zone integration. To investigate the effect of disorder structure on the Cr_2FeGa alloy, a $2 \times 2 \times 2$ supercell containing 32 atoms was created, and the $8 \times 8 \times 8$ k-point setting was adopted for Brillouin zone integration. The Korringa-Kohn-Rostoker Green's function method is also employed, which is combined with the coherent potential approximation [25–27]. Furthermore, we investigate the intrinsic anomalous Hall conductivity (AHC) of the alloys induced by Berry curvature. The Bloch wave functions are projected into a maximally localized Wannier function to obtain the tight-binding model Hamiltonian, and AHC was calculated in the evaluation of the integrals [28–30]. The s and p orbitals for Ga and the d orbitals for Co, Cr, and Fe are included to obtain the precise Wannier functions. The intrinsic AHC (σ_{xy}^{int}) is calculated in the tight-binding models constructed from these Wannier functions and can be expressed as [31],

$$\sigma_{xy}^{int} = \frac{e^2}{\hbar} \int \frac{d\boldsymbol{k}}{(2\pi)^3} \Omega_z(\boldsymbol{k}) f(\boldsymbol{k}),$$

where $\Omega_z(\boldsymbol{k})$ is the z component of Berry curvature for $\boldsymbol{k}$, and $f(\boldsymbol{k})$ represents the Fermi distribution function.

All the possible structures for the three alloys are considered in the calculations and the most stable structure is given in the paper. The Heusler alloy Co_2FeGa ($x = 0$) crystallizes in the $L2_1$ phase, as shown in Fig. 1(a). Taking all symmetries into consideration, CoCrFeGa ($x = 1$) exhibits three distinct possible site occupations, with Co, Cr, Fe, and Ga atoms arranged along the diagonal of the fcc cube in the order of A-B-C-D, A-C-B-D, and A-B-D-C. We have investigated all structures and found that the first ordering A-B-C-D is the most stable, as shown in Fig. 1(b), which is consistent with the previous study [32], while Cr_2FeGa ($x = 2$) is found to be the XA phase, as illustrated in Fig. 1(c). The calculated equilibrium lattice constants are 5.719, 5.720, and 5.783 Å for Co_2FeGa, CoCrFeGa, and Cr_2FeGa, respectively, increasing with the replacement of Co by Cr.

III. RESULTS AND DISCUSSION

A. Band structure regulation

The spin-resolved band structure and partial density of states (PDOS) of Co_2FeGa are shown in Fig. 2. It can be found that the bands across the E_F in both the spin-down and the spin-up states, indicating the metallic properties of the alloy [see Fig. 2(a)]. Although there is no gap in the spin-down direction, the overlap between the valence band maximum and the conduction band minimum is only 0.06 eV at the G and X points. As a result, a wide pseudogap is formed at E_F, as evidenced by the DOS [see Fig. 2(b)]. There are only several bands across the E_F for the spin-up direction, resulting in a flat and very low DOS value near the E_F. It should be noticed that E_F falls into the pseudogap in the spin-down channel while a small finite value for the spin-up one
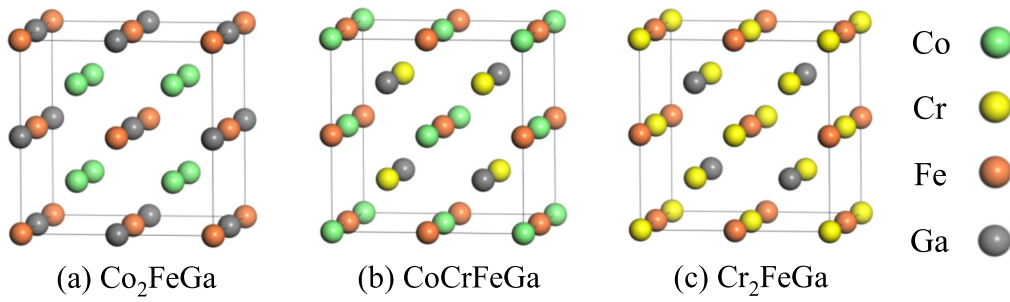
FIG. 1. Crystal structure in unit cell for $Co_{2-x}Cr_xFeGa$ with (a) $x = 0$, (b) $x = 1$, and (c) $x = 2$.

which makes spin polarization of Co_2FeGa only have 63%. The PDOS reveals a clear exchange splitting between the spin-up and spin-down directions, suggesting the FM property [see Fig. 2(b)].

It should be noticed from Fig. 2(b) that there is an obvious pseudogap in the spin-up direction from -1.5 to -1.2 eV at below E_F. The DOS of Co_2FeGa is sketched, as shown in Fig. 2(c). If we move the E_F of the spin-up channel into the narrow pseudogap without destroying the wide pseudogap in the spin-down channel, we can open a zero-width energy gap at E_F in the spin-up direction. This results in an SGS, as depicted in Fig. 2(d). If we continue to lower the E_F of the spin-up channel to a higher DOS while still keeping the E_F within the pseudogap of the spin-down direction, a near HM
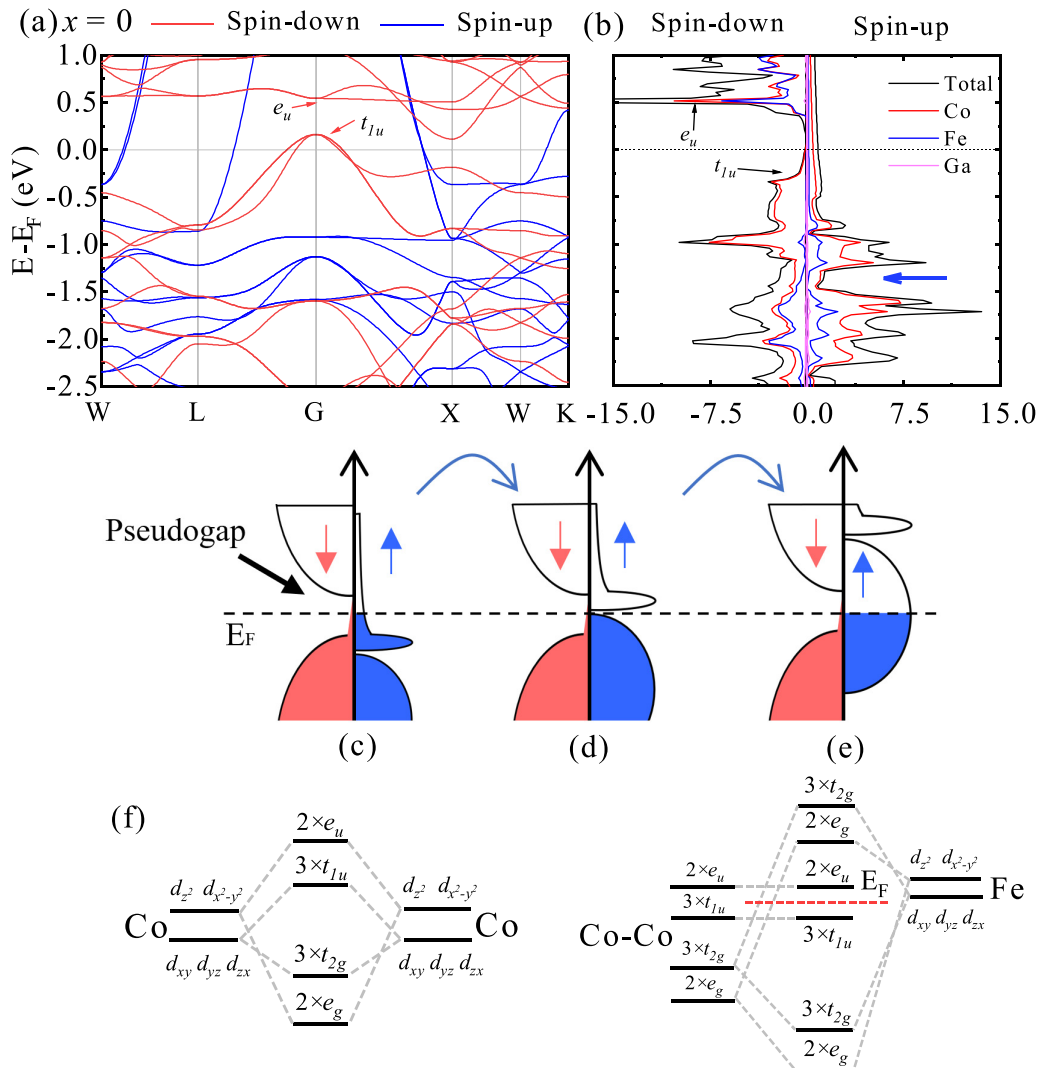
FIG. 2. Spin-resolved (a) band structure; (b) total DOS and PDOS of Co_2FeGa. The schematic DOS of (c) FM metal, (d) FIM SGS, and (e) near FIM HM. (f) The schematic diagram of spin-down orbital hybridization of Co_2FeGa. The red dashed line is Fermi level.

state will be formed. This enhances the spin polarization of the sample, as shown in Fig. 2(e).

To illustrate the origin of the band gap in the spin-down direction and guide us to tune the E_F in the spin-up direction, a schematic diagram of the spin-down orbital hybridization of Co_2FeGa is provided [see Fig. 2(f)]. The d orbitals of transition metal elements contribute significantly to the DOS around E_F. Therefore, the s and p orbitals, as well as the orbitals of the main group element Ga are not considered. The hybridization between the A and C sites of the Co-Co atoms are first considered. The d orbitals of the Co atom split into triple degenerate d_{xy}, d_{yz}, and d_{zx} orbitals and double degenerate d_{z^2} and $d_{x^2-y^2}$ orbitals. The d_{xy}, d_{yz}, and d_{zx} orbitals of the two Co atoms hybridize with each other to form the triple degenerate t_{2g} bonding orbital and the t_{1u} antibonding orbital, while the d_{z^2} and $d_{x^2-y^2}$ orbitals form the double degenerate e_g bonding orbital and the e_u antibonding orbital [see the left side of Fig. 2(f)]. As depicted in the right side of Fig. 2(f), the t_{2g} and e_g bonding orbitals of Co-Co hybridize with Fe's triple degenerate d_{xy}, d_{yz}, and d_{zx} orbitals and the double degenerate d_{z^2} and $d_{x^2-y^2}$ orbitals, eventually forming the bonding orbitals t_{2g} and e_g with the lower energy and antibonding orbitals t_{2g} and e_g with higher energy. As the requirement of the high symmetry of the crystal structure, the antibonding orbitals e_u and t_{1u} of Co-Co maintain the energy level as they cannot hybridize with the Fe atom, which is corresponding to the absence of the Fe component in the spin-down channel DOS from -1 to 0.2 eV [see Fig. 2(b)].

The primitive cell of Co_2FeGa contains 29 valence electrons, while hybridized e_g, t_{2g}, t_{1u}, as well as the s and p orbitals of the Ga atom can hold 24 electrons in total. Therefore, E_F falls within the gap between t_{1u} and e_u of minority states. This is evident in the DOS diagram for the spin-down direction, as shown in Fig. 2(b). The remaining five electrons fill the orbitals of e_u (two electrons), e_g (two electrons), and t_{2g} (one electron) of the spin-up direction, and this filling rule of electrons can be found in some other $L2_1$ ferromagnetic Co_2-based Heusler alloys with 29 valence electrons, such as Co_2MnGe [33], Co_2MnSn [33], and Co_2FeAl [34]. So the triple degenerated t_{2g} antibond orbitals are corresponding to the flat and low DOS around the E_F of Co_2FeGa in the spin-up direction [see Fig. 2(b)]. Therefore, in order to change it into a SGS, we can adjust the E_F the in spin-up direction to fall between two orbitals, i.e., between e_u and e_g, by reducing three valence electrons. Cr has three valence electrons less than Co, so Cr was chosen to replace Co to tune the E_F in this study. If further replacing another Co with Cr, we can adjust the E_F into hybridized antibonding orbitals t_{1u} and e_u with high DOS to form a HM.

Figure 3 shows the band structure and DOS of $Co_{2-x}Cr_xFeGa$ for $x = 1$ and 2. Compared with Co_2FeGa, the band structure in spin-down direction does not change much; however, there is a large change in the spin-up direction. For $x = 1$, the spin-up E_F moves towards lower energy by about 1 eV, exactly falling into a narrow gap, in which the top of the valence band and the bottom of the conduction band almost touch each other, and they only overlap by 0.02 eV at the L and X points [see Fig. 3(a)]. Additionally, there is a gap of 0.02 eV just above E_F in the spin-down direction, which is also evident by the DOS of CoCrFeGa shown in Fig. 3(b), suggesting
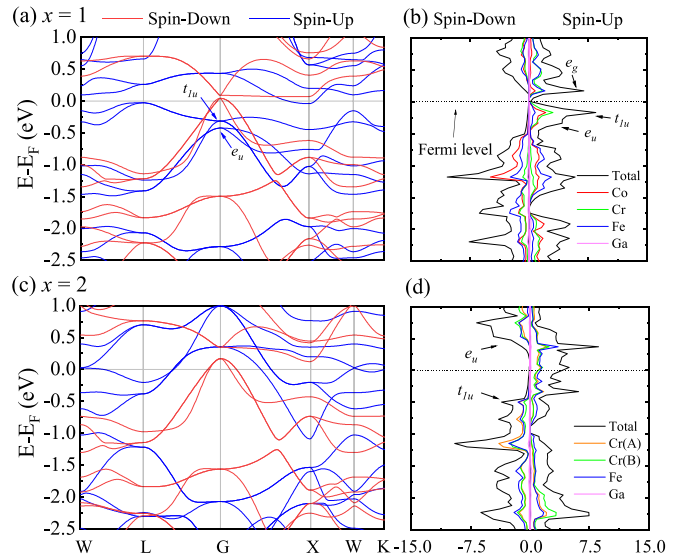

FIG. 3. Spin-resolved band structure, total DOS, and PDOS of $Co_{2-x}Cr_xFeGa$ for (a) and (b) $x = 1$, and (c) and (d) $x = 2$.

the near SGS character. Cr has three valence electrons less than Co, and the valence electron number of the compound CoCrFeGa is 26. Consequently, the original occupied orbitals of t_{2g} and e_g in the spin-up directions for Co_2FeGa will be unoccupied, resulting in that the E_F moves towards lower energy and eventually falls into the small pseudogap between the e_g and t_{1u} orbitals described earlier. Hence a near SGS forms in CoCrFeGa. This is also the reason why Heusler alloys with a valence electron count of 26, i.e,. Mn_2CoAl [35], CoFeCrAl, and CoMnCrSi [36], tend to form a SGS. It can be seen that the exchange splitting between the spin-up and down reduces a lot compared with Co_2FeGa. In fact, there is a parallel arrangement of magnetic moments between Co and Fe atoms, while an antiparallel arrangement between Cr and Fe (Table I), which leads to a FIM property in CoCrFeGa.

For $x = 2$, one more Cr replacing Co leads to a change in composition to Cr_2FeGa with a valence electron number of 23. The band structure shown in Fig. 3(c) indicates that the spin-up band goes beyond the spin-down band in energy, which is due to less valence electrons in the spin-up direction compared to the spin-down direction. As shown in Fig. 3(d), the DOS of Cr_2FeGa keeps the pseudogap position of the spin-down direction, while the spin-up E_F is adjusted into the high DOS region of the t_{1u} and e_u orbitals formed by Cr-Fe hybridization, resulting in a high spin polarization of 95%. The PDOS in Fig. 3(d) demonstrates nearly equal contributions from the Cr(A), Cr(B), and Fe atoms, indicating the strong hybridization among them.

The calculated formula moment, atomic moment, and the spin polarization are shown in Table I. The formula moments of Co_2FeGa, CoCrFeGa, and Cr_2FeGa are 5.07, 1.97, and 0.96 μ_B/f.u., respectively, almost obeying the Slater-Pauling rule of $M = N_V - 24$, where M is the formula moment and N_V is the number of valence electrons. A slight deviation to the integer magnetic moment is attributed to a band crossing in the spin-down direction at E_F. Obviously, there is a ferromagnetic exchange coupling between Co and Fe in Co_2FeGa

TABLE I. Calculated formula moment M_{tot}, each atomic moment M (μ_B/f.u.), and spin polarization (%) of $Co_{2-x}Cr_xFeGa$ ($x = 0$, 1, and 2).

Compounds	M_{tot}	M_{Co}	$M_{Cr(A)}$	$M_{Cr(B)}$	M_{Fe}	M_{Ga}	Spin polarization (%)
Co_2FeGa	5.07	1.18			2.77	−0.07	63
$CoCrFeGa$	1.97	0.94		1.80	−0.73	−0.04	77
Cr_2FeGa	0.96		1.62	−1.33	0.67	0.01	95

and forms the ferromagnetic moment arrangement, which is consistent with previous study by Liu and Altounian [37]. However, in XA-type Mn_2CuGe with the same valence count of 29, there is a strong antiparallel coupling between two Mn atoms, which leads to a different electron occupation in the spin-down channel [38]. This makes it a FIM material with a magnetic moment of 0.97 μ_B/f.u., which obeys a different Slater-Pauling rule of $M = N_V - 28$ [39]. In $CoCrFeGa$, there is an antiparallel coupling between Cr and Fe atoms, but a parallel coupling between Co and Cr atoms, forming a FIM SGS. As for Cr_2FeGa, $Cr(A)$, and $Cr(B)$ atoms, as well as Fe and $Cr(B)$ atoms, both form antiparallel coupling, resulting in a significant decrease in formula moment. It can be found that by gradually replacing Co with Cr in Co_2FeGa, the transition from FM metal to near FIM SGS to near FIM half-metal has been achieved.

Figure 4 displays the energy-dependent intrinsic AHC (σ_{xy}^{int}) of $Co_{2-x}Cr_xFeGa$ ($x = 0$, 1, and 2) calculated with Wannier functions. In this study, we consider the magnetization along the z direction and present the intrinsic AHC in the xy plane. Our results show that the intrinsic AHC at E_F is 128 S/cm for $x = 0$ and 162 S/cm for $x = 1$. For $x = 2$, the intrinsic AHC at E_F is calculated to be 366 S/cm, but there is a compensation point located just 0.06 eV above E_F, which leads to an unstable AHC. As a result, a small impurity or disorder structure in the sample may shift E_F, resulting in a sudden decrease in the AHC experimentally. Overall, it can be concluded that the intrinsic AHC of the well-ordered $Co_{2-x}Cr_xFeGa$ alloys is enhanced with increasing x.

B. Experimental results

The XRD patterns for the $Co_{2-x}Cr_xFeGa$ ($x = 0$, 1, and 2) powder samples were measured at room temperature and

are shown in Fig. 5(a). To clearly observe the superlattice peaks, a step scan mode with the step size of 0.02° and 3 s step time was used to measure the diffraction peaks in the range of 20°–40°, as shown in the inset of Fig. 5(a). The main peaks of (220), (400), and (422) indicate the body-centered cubic structure of three samples and the superlattice peak of (200) is observed. However, the superlattice peak of (111) is absent for all three samples. The experimental lattice constants obtained by Bragg's law are 5.74, 5.78, and 5.86 Å for $x = 0$, 1, and 2, respectively, which are a little larger than those calculated by first-principles calculations, with the average deviations ~1%. The structure factors of superlattice peaks (111) and (200) in the Heusler alloy are as follows [40]: $F_{111} = |4[(f_A - f_C)^2 + (f_B - f_D)^2]|^{1/2}$ and $F_{200} = 4|f_A - f_B + f_C - f_D|$, where f is the scattering factor of the atom depending on the type of element. Because of the similar scattering factors of the constituent elements of Cr, Co, and Fe [41], disorder between the B and D sites leads to the disappearance of the superlattice peak of (111). In fact, it has been confirmed that atomic swap disorder between the B and D sites is common in Heusler structures. Thus, the absence of superlattice peak (111) indicates disorder between the B and D sites.

Rani *et al.* conducted first-principles calculations on disorder and discovered that the SGS nature of $CoFeCrGa$ is highly resistant to Co-Fe swap disorder. However, when the swap disorder between Cr (B site) and Ga (D site) exceeds 25%, the system switches from SGS to a half-metallic state [42]. As no disorder calculation of Cr_2FeGa was performed in previous studies, we also conduct calculations on different kinds of disorder in Cr_2FeGa, and it is found that the disorder between Cr (B site) and Ga (D site) leads to the most stable structure (refer to Supplemental Material Fig. S1 [43]).
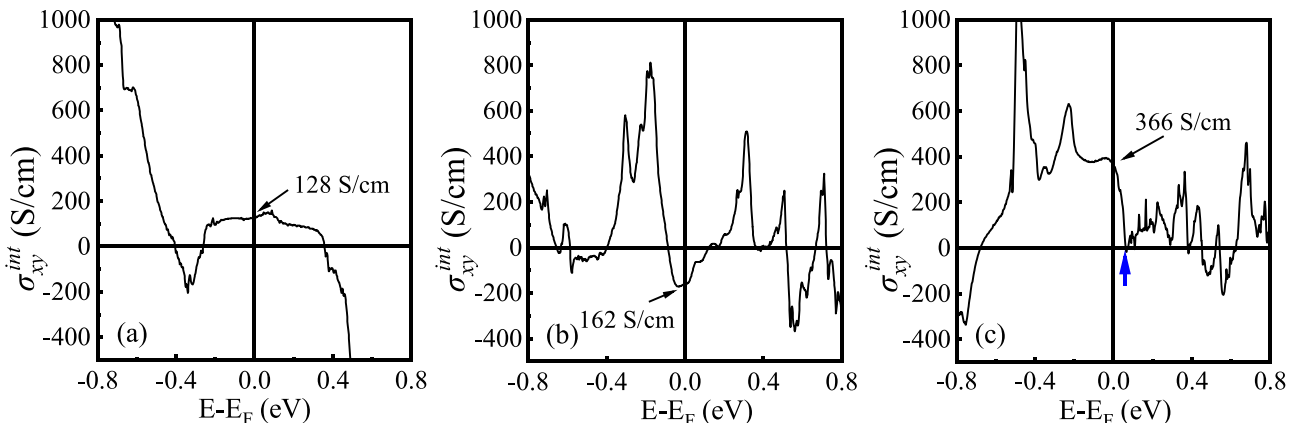
FIG. 4. Energy dependence intrinsic AHC (σ_{xy}^{int}) of $Co_{2-x}Cr_xFeGa$ for (a) $x = 0$, (b) $x = 1$, and (c) $x = 2$.
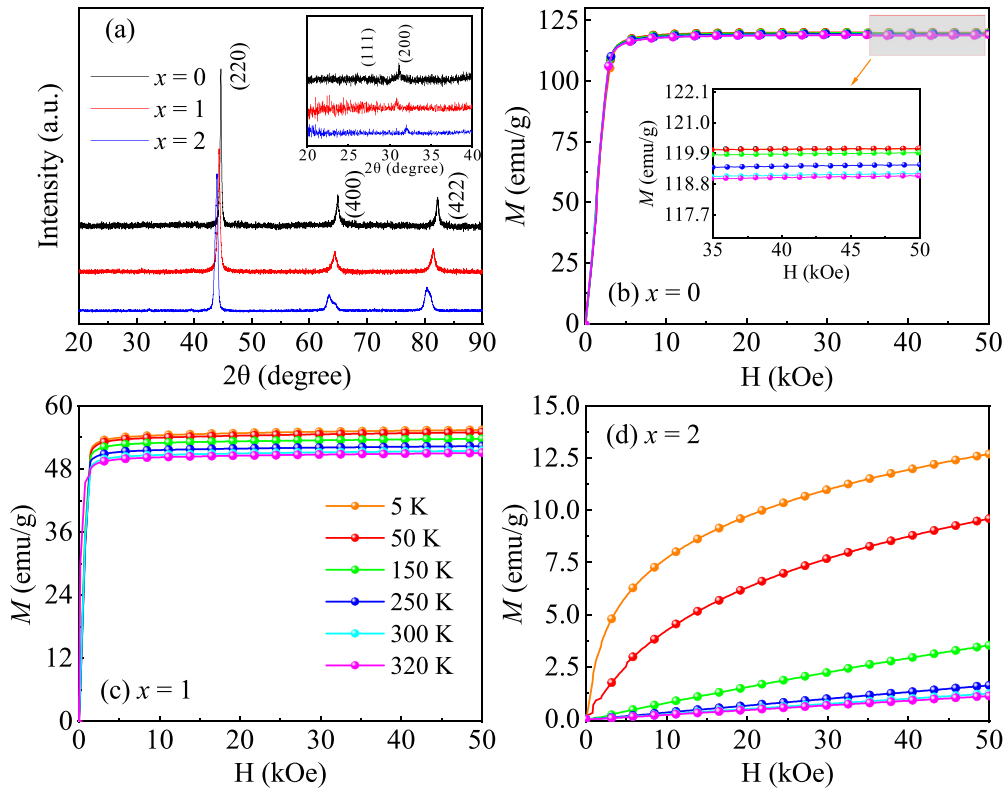
FIG. 5. (a) Room-temperature XRD patterns of $Co_{2-x}Cr_xFeGa$ ($x = 0$, 1, and 2). Inset shows the diffraction peaks in the range of 20°–40° measured by using step scan mode. Magnetic field dependence of magnetization at different temperatures for (b) $x = 0$, (c) $x = 1$, and (d) $x = 2$. The inset in (b) shows the details at high field.

Interestingly, spin polarizations of 93.7% and 98.9% were obtained with disorder levels of 12.5% and 50%, respectively (see Supplemental Material Fig. S2 [43]). Hence, real samples can be considered as SGSs for CoCrFeGa and half-metals for Cr_2FeGa.

Isothermal magnetization curves of the three alloys obtained under magnetic field (0–50 kOe) were shown in Fig. 5. The magnetization of Co_2FeGa saturates at a small field of about 5 kOe at 5 K. The saturation magnetization (M_S) is derived to be 119.9 emu/g (5.21 μ_B/f.u) by linear extrapolation of the magnetization at high field. As can be seen in the inset of Fig. 5(b), the M_S in a wide temperature range (5–320 K) varies little, suggesting the T_C of Co_2FeGa is much higher than room temperature. This is consistent with the previous report that the T_C of Co_2FeGa is above 1100 K [20].

As shown in Fig. 5(c), the CoCrFeGa alloy reaches saturation at 3 kOe at 5 K with an extrapolated M_S value of 54.33 emu/g (2.25 μ_B/f.u.), which is slightly higher than the theoretically calculated value of 1.97 μ_B/f.u. As the temperature increases to 320 K, M_S gradually decreases to 49.8 emu/g (2.06 μ_B/f.u.). This saturation behavior suggests a T_C much higher than 320 K, which is in line with the previously reported high value of 686 K [41]. The magnetization of Cr_2FeGa shown in Fig. 5(d) drops rapidly from 150 K due to its relative low T_C and shows an unsaturated state with a field of 0–50 kOe. The extrapolated value of M_S is 8.70 emu/g (0.36 μ_B/f.u.), which is smaller than the theoretical calculation value of 0.96 μ_B/f.u. This obvious reduction is attributed to the swap disorder in the sample. In the isostructural

alloy Cr_2CoGa, which has one electron more than Cr_2FeGa, it is theoretically calculated to be a fully compensated FIM half-metal with the magnetic moment close to zero, while the experiment shows the moment of Cr_2CoGa is 0.46 μ_B/f.u. [44]. The theoretical calculation suggested that atomic disorder between Cr(B)-Co has an obvious influence on the magnetization [45].

The temperature dependence of longitudinal resistivity (ρ_{xx}) for the $Co_{2-x}Cr_xFeGa$ alloys was measured from 350 to 5 K with zero magnetic field as shown in Fig. 6. We found that the ρ_{xx} of Co_2FeGa increases from 5.9 to 21 $\mu\Omega$ cm with the increase of temperature, exhibiting a metallic behavior, which is consistent with the previous study by Zhang *et al.* [46]. To figure out the component of the temperature dependence resistivity, the Matthiessen's rule [47], $\rho_{xx}(T) = \rho_0 + \rho_{e-p}(T) + \rho_{e-m}(T)$, for metallic alloys is used. Here ρ_0, ρ_{e-p}, and ρ_{e-m} represent residual resistivity, linear temperature-dependent electron-phonon scattering component, and quadratic temperature-dependent electron-magnon scattering component, respectively. In the temperature range of 5–100 K, as shown in Fig. 6(a), $\rho_{xx}(T)$ can be fitted as quadratic temperature dependence $\rho = \rho_0 + bT^2$ with $\rho_0 = 5.80 \ \mu\Omega$ cm and coefficient $b = 3.37 \times 10^{-4} \ \mu\Omega$ cm K^{-2} while the coefficient of the linear term is close to zero, showing that the variation of longitudinal resistivity in the low temperatures is dominated by electron-magnon scattering. The residual resistivity ratio (RRR = ρ_{300}/ρ_0) of Co_2FeGa is calculated to be 3.11. In temperatures ranging from 100 to 350 K, a combination of linear and quadratic temperature depen-
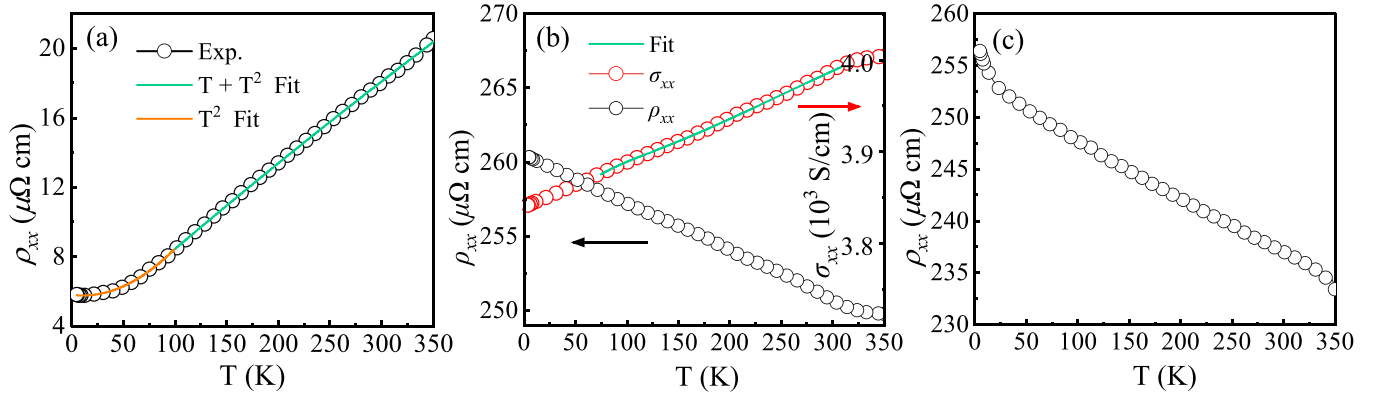
FIG. 6. Temperature dependence of resistivity (ρ_{xx}) of alloys $Co_{2-x}Cr_xFeGa$ for (a) $x = 0$, (b) $x = 1$ along with longitudinal conductivity (σ_{xx}), and (c) $x = 2$ in zero field.

dence can fit well with the coefficient to be $0.052\ \mu\Omega\ cm\ K^{-1}$ and $-1.11 \times 10^{-5}\ \mu\Omega\ cm\ K^{-2}$, respectively. The fitting coefficient of the linear term is negative and much smaller than that of the quadratic term, showing that the variation of resistivity is dominated by electron-phonon rather than electron-magnon scattering in high temperatures.

The temperature dependencies of the electric resistivity and conductivity of CoCrFeGa ($x = 1$) are shown in Fig. 6(b). The curve appears to exhibit semiconductorlike behavior with a negative temperature coefficient of resistance (TCR). For the CoCrFeGa alloy, the longitudinal resistivity mildly drops from 262 to 251 $\mu\Omega$ cm in the temperature ranging from 5 to 350 K. The small resistivity variation is due to the smaller gap at the E_F of the SGS property compared with a typical semiconductor. Due to the zero gap at the E_F of CoCrFeGa, the charge carriers can be easily excited at low temperature, and the sample is expected to display negative TCR, similar to gapless semiconductors. The linear decrease behavior of resistivity is also observed in the SGS materials Mn_2CoAl [35] and CrVTiAl [48]. Figure 6(b) also shows the conductivity of CoCrFeGa. A two-carrier model is employed to investigate the gapless behavior and linear variation [49],where the temperature-dependent conductivity can be given by

$$\sigma(T) = \sigma_e + \sigma_h = A_e(T)e^{-(\Delta E_e/k_BT)} + A_h(T)e^{-(\Delta E_h/k_BT)},$$

where $A_i(T) = en_{i0}\mu_{i0}/(1 + a_iT)$ for $i = e$ and h, and the e and h represent electron and hole, respectively. The n_{i0} and μ_{i0} represent the carrier concentration and mobility at 0 K, respectively, and a_i corresponds to electron-phonon scattering. The data from 75–300 K is fitted with this model, as shown by the green line in Fig. 6(b). The best parameters of ΔE_e and ΔE_h fitted are 146 and 0.29 meV, respectively. It is found that $A_i(T)$ for both the electron and the hole hardly change with temperature, with values of approximately 493 and 3923 S/cm, respectively. The temperature parameter a_i is fitted to be close to zero. The σ_e and σ_h are fitted to be 76 and 3910 S/cm at 300 K, respectively. As the σ_e is much smaller than the σ_h, the transport behavior in CoCrFeGa is dominated by holes.

The ρ_{xx} of Cr_2FeGa also decreases from 256 to 230 $\mu\Omega$ cm in the temperature range of 5–350 K, as shown in Fig. 6(c). There is a distinct turning point near T_C and the

slope decreases as the temperature increases. The linear decrease of resistivity indicates the lack of the $\rho_{e-m}(T)$ term, the quadratic temperature-dependent electron-magnon scattering component. The magnon scattering is a spin-flip process, and the lack of electron-magnon interactions indicates a lack of minority spin electrons in the E_F. Mott *et al.* proposed that localization of electrons can occur when the E_F is located in a deep gap or pseudogap [50]. The localization of charge carriers in the Cr_2FeGa may cause a negative TCR. Additionally, in some alloys, such as Co_2CrAl, the disordered sample also exhibits lower negative TCR values than the ordered one [51]. So, swap disorder may be another reason for the negative TCR for Cr_2FeGa. It can be seen that the resistivity change of Cr_2FeGa is consistent with the rule of Mooij [52], that metallic materials with resistivity above 100–200 $\mu\Omega$ cm typically exhibit a negative TCR while those with resistivity below 100–200 $\mu\Omega$ cm usually exhibit a positive TCR.

Figures 7(a) and 7(b) show the magnetic field dependence of transverse Hall resistivity ρ_{xy} of CoCrFeGa and Cr_2FeGa at different temperatures. Since the longitudinal resistivity is too small, resulting in the Hall signal of Co_2FeGa being too weak to observe, no Hall data is shown here. As can be seen in Fig. 7(a), for the CoCrFeGa alloy, ρ_{xy} increases linearly in the low field range, and varies very little after saturation. It is evident that the saturation ρ_{xy} decreases slowly from 3.51 to 3.2 $\mu\Omega$ cm with the increase of temperature from 5 to 320 K in CoCrFeGa, while ρ_{xy} decreases rapidly in Cr_2FeGa. The Hall resistivity ρ_{xy} originates from the ordinary Hall resistivity (ρ_{xy}^O) and the anomalous Hall resistivity (ρ_{xy}^A), which is expressed to be $\rho_{xy} = \rho_{xy}^O + \rho_{xy}^A = R_0H + R_sM$, here ρ_{xy}^O is associated with the Lorentz force and is expressed as the product of the ordinary Hall coefficient (R_0) and the applied magnetic field (H). Meanwhile, ρ_{xy}^A is proportional to magnetization (M) with an anomalous Hall coefficient (R_s). By linearly extrapolating the high field ρ_{xy} to zero field, we can determine the intercept and slope, which correspond to ρ_{xy}^A and R_0, respectively. The carrier concentration (n) can be calculated from R_0 using the equation $n = \frac{1}{eR_0}$, which is a function of temperature. The n varies from 1.08 to $1.4 \times 10^{21}\ cm^{-1}$ as the temperature ranges from 5 to 320 K (see Supplemental Material Fig. S3 [43]). The nearly temperature-independent behavior of the carrier concentration indicates the
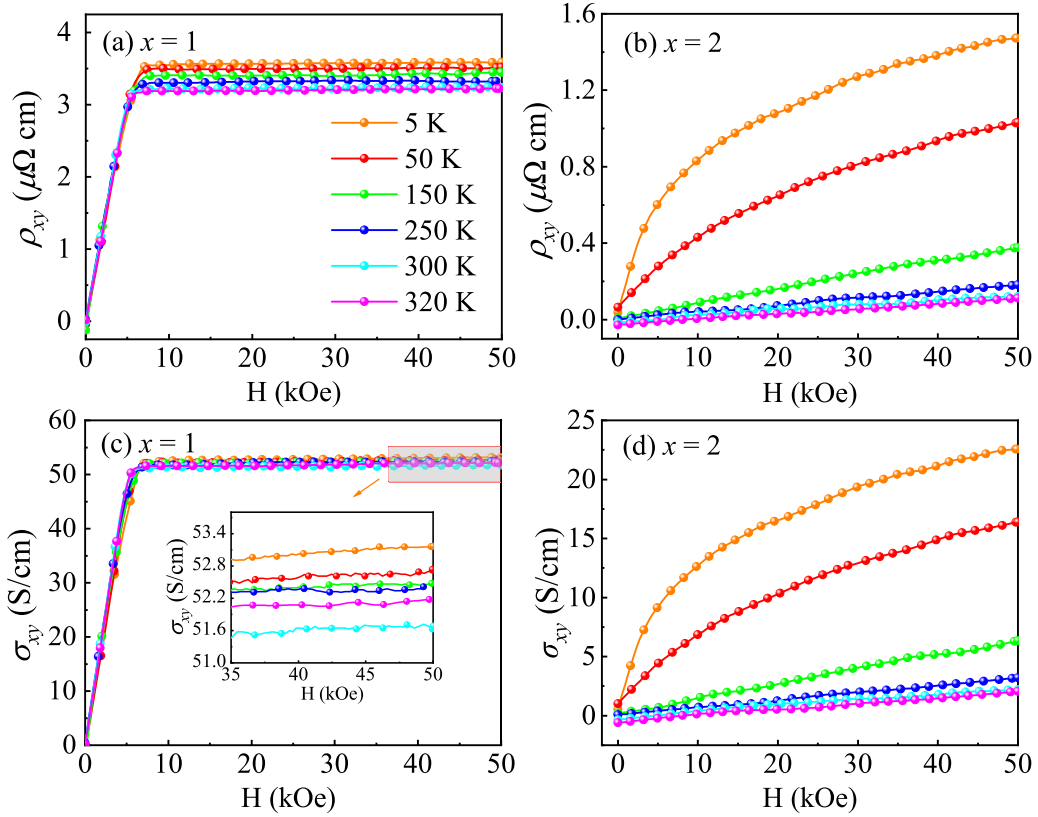
FIG. 7. Magnetic field dependence of the Hall resistivity (ρ_{xy}) for Co$_{2-x}$Cr$_x$FeGa alloys with (a) $x = 1$, (b) $x = 2$, and Hall conductivity (σ_{xy}) for (c) $x = 1$ and (d) $x = 2$.

SGS property of CoCrFeGa [53]. The field dependence Hall conductivity σ_{xy} shown in Figs. 7(c) and 7(d) is calculated by $\sigma_{xy} = \frac{\rho_{xy}}{\rho_{xx}^2 + \rho_{xy}^2}$. As ρ_{xy}^2 is much smaller than ρ_{xx}^2, this formula can be expressed as $\sigma_{xy} = \frac{\rho_{xy}}{\rho_{xx}^2}$. For CoCrFeGa, the AHC σ_{xy}^A is determined by extrapolating σ_{xy} of high field to zero field [see Fig. 8(b)]. The σ_{xy}^A is considered to be contributed by the extrinsic (σ_{xy}^{ext}) and intrinsic (σ_{xy}^{int}) parts ($\sigma_{xy}^A = \sigma_{xy}^{ext} + \sigma_{xy}^{int}$), and shows a slight decrease with the increase of temperature. The value of σ_{xy}^A at 5 K is found to be a small value of 52.7 S/cm, which is comparable to the value of the AHC reported in the other SGSs, such as 27 S/cm in Mn$_2$CoAl at 2 K [54] and 20 S/cm in CoFeTiSn at 5 K [55].

To shed light on the origin of the observed AHE in CoCrFeGa, we employ a scaling model reported by Tian *et al.* [56]: $\rho_{xy}^A = a\rho_{xx0} + b\rho_{xx}^2$. The first term, $a\rho_{xx0} = \alpha\rho_{xx0} + \beta\rho_{xx0}^2$, represents the extrinsic component which includes skew scattering parameter α and side jump scattering parameter β with a constant residual resistivity $\rho_{xx0} = 261.29\ \mu\Omega$ cm. The parameter b in the second term represents the intrinsic component associated with the integration of momentum-space Berry curvature. The value of ρ_{xy}^A exhibits a linear relationship with ρ_{xx}^2. This relationship is depicted in Fig. 8(a) through a linear fitting curve represented by the above equation. The fitted parameter a is determined to be -0.288×10^{-2}, and the intrinsic parameter b is found to be 63.23 S/cm, which is consistent with the calculated value 162 S/cm by the order of magnitude. The relatively small intrinsic component b suggests that CoCrFeGa possesses the SGS property. Specifically, in an SGS, the characteristic band structure results in a compensation point of AHC around E_F by two opposite spin directions, leading to a small observed intrinsic component of AHC [57]. In off-stoichiometric Co$_{1-x}$Fe$_{1-x}$CrGa compounds, the intrinsic components are derived to be 69 and 94 S/cm for $x = 0.1$ and 0.3, respectively, which increases with deviating from the stoichiometric CoCrFeGa [41]. The negative value a suggests the extrinsic component gives rise to the AHE in an opposite way as the intrinsic component. Employing the equation $\sigma_{xy}^A = \sigma_{xy}^{ext} + \sigma_{xy}^{int}$, the extrinsic contribution to AHC (σ_{xy}^{ext}) is estimated, and the
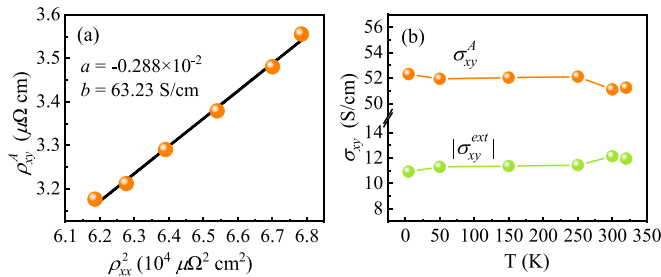

FIG. 8. (a) The linear fitting curve of ρ_{xy}^A vs ρ_{xx}^2 for CoCrFeGa. (b) The temperature dependence of σ_{xy}^A and extrinsic component $|\sigma_{xy}^{ext}|$ for CoCrFeGa.

temperature dependence of $|\sigma_{xy}^{ext}|$ is shown in Fig. 8(b). Obviously, the $|\sigma_{xy}^{ext}|$ is smaller than the intrinsic one in the whole temperature range, and increases slightly with temperature.

For Cr$_2$FeGa shown in Fig. 7(d), the field-dependent Hall conductivity σ_{xy} shows a similar trend as the ρ_{xy}-H curve. The maximum of the value of σ_{xy}^A is 14.1 S/cm at 5 K, which is rather small compared with the calculated one (366 S/cm). The disorder structure discussed before may change the band structure slightly and induces a movement of E_F, resulting in the great decrease of intrinsic AHC. Above 150 K, σ_{xy} shows a linear field dependence, which is due to the absence of magnetism when the temperature is higher than T_C.

IV. CONCLUSION

In conclusion, Heusler alloys Co$_{2-x}$Cr$_x$FeGa ($x = 0$, 1, and 2) have been studied theoretically and experimentally from the aspect of electronic structure, magnetism, and anomalous transport properties. First-principles calculations suggest a transition from FM to near FIM SGS to near FIM HM is realized and an enhancement of spin polarization is achieved by replacing Co with Cr gradually. The ferromagnetic Co$_2$FeGa alloy has a low P (63%) with an observed saturation moment of 5.21 μ_B/f.u. at 5 K. The longitudinal resistivity of Co$_2$FeGa exhibits metallic property, increasing from 5.9 to 21 $\mu\Omega$ cm from 5 o 350 K. Replacing one Co atom with Cr results in a near SGS property in CoCrFeGa because the E_F in the spin-up channel is adjusted into a narrow gap. The AHE has been extensively studied both theoretically and

experimentally. According to calculations, the intrinsic AHC induced by the Berry curvature is found to increase from 128 to 366 S/cm with doping Cr in ordered Co$_{2-x}$Cr$_x$FeGa. The AHE was also experimentally studied in CoCrFeGa, and a maximum σ_{xy}^A of 52.7 S/cm was observed at 5 K and it is found that both intrinsic and extrinsic factors are responsible for the AHE. When further doping another Co with Cr, namely, in Cr$_2$FeGa, the enhancement of P (95%) was achieved due to the proper tuning of the E_F in the spin-up channel, creating an almost half-metallic metal. The compound Cr$_2$FeGa, as well as CoCrFeGa, exhibits a semiconductorlike behavior with a negative TCR in temperature ranging from 5 to 350 K. The experimental saturated formula moment of Cr$_2$FeGa exhibits the maximum value (0.36 μ_B/f.u.) at 5 K deviating from the calculated value (0.96 μ_B/f.u.), which is attributed to the disorder in the sample. In addition, a small σ_{xy}^A (14.1 S/cm) of Cr$_2$FeGa is observed at 5 K. As the temperature increases above 150 K, the saturated formula moment as well the AHC becomes zero. The scheme of modulating the position of the E_F to achieve the FM→near FIM SGS→near FIM HM transition is proposed in this work. The enhanced spin polarization provides an opportunity for spintronics application.

[1] R. A. de Groot, F. M. Mueller, P. G. van Engen, and K. H. J. Buschow, New class of materials: Half-metallic ferromagnets, Phys. Rev. Lett. **50**, 2024 (1983).

[2] G. E. Rowlands, S. V. Aradhya, S. Shi, E. H. Yandel, J. Oh, D. C. Ralph, and R. A. Buhrman, Nanosecond magnetization dynamics during spin Hall switching of in-plane magnetic tunnel junctions, Appl. Phys. Lett. **110**, 122402 (2017).

[3] S. Bhatti, R. Sbiaa, A. Hirohata, H. Ohno, S. Fukami, and S. N. Piramanayagam, Spintronics based random access memory: A review, Mater. Today **20**, 530 (2017).

[4] A. Sakai, Y. P. Mizuta, A. A. Nugroho, R. Sihombing, T. Koretsune, M. T. Suzuki, N. Takemori, R. Ishii, D. Nishio-Hamane, R. Arita, P. Goswami, and S. Nakatsuji, Giant anomalous Nernst effect and quantum-critical scaling in a ferromagnetic semimetal, Nat. Phys. **14**, 1119 (2018).

[5] P. G. Li, J. Koo, W. Ning, J. G. Li, L. X. Miao, L. J. Min, Y. L. Zhu, Y. Wang, N. Alem, C. X. Liu, Z. Q. Mao, and B. H. Yan, Giant room temperature anomalous Hall effect and tunable topology in a ferromagnetic topological semimetal Co$_2$MnAl, Nat. Commun. **11**, 3476 (2020).

[6] E. K. Liu, Y. Sun, N. Kumar, L. Muechler, A. Sun, L. Jiao, S. Y. Yang, D. Liu, A. Liang, Q. N. Xu, J. Kroder, V. Süß, H. Borrmann, C. Shekhar, Z. S. Wang, C. Y. Xi, W. H. Wang, W. Schnelle, S. Wirth, Y. L. Chen, S. T. B. Goennenwein, and C. Felser, Giant anomalous Hall effect in a ferromagnetic kagome-lattice semimetal, Nat. Phys. **14**, 1125 (2018).

[7] M. I. Katsnelson, V. Y. Irkhin, L. Chioncel, A. I. Lichtenstein, and R. A. de Groot, "Half-metallic ferromagnets: From band structure to many-body effects," Rev. Mod. Phys. **80**, 315 (2008).

[8] S. M. Griffin and J. B. Neaton, Prediction of a new class of half-metallic ferromagnets from first principles, Phys. Rev. Mater. **1**, 044401 (2017).

[9] J. Kubler, G. H. Fecher, and C. Felser, Understanding the trend in the Curie temperatures of Co$_2$-based Heusler compounds: *Ab initio* calculations, Phys. Rev. B **76**, 024414 (2007).

[10] G. Qin, W. Ren, and D. J. Singh, Interplay of local moment and itinerant magnetism in cobalt-based Heusler ferromagnets: Co$_2$TiSi, Co$_2$MnSi and Co$_2$FeSi, Phys. Rev. B **101**, 014427 (2020).

[11] S. Chernov, C. Lidig, O. Fedchenko, K. Medjanik, S. Babenkov, D. Vasilyev, M. Jourdan, G. Schönhense, and H. J. Elmers, Band structure tuning of Heusler compounds: Spin- and momentum-resolved electronic structure analysis of compounds with different band filling, Phys. Rev. B **103**, 054407 (2021).

[12] P. Chaudhary, K. K. Dubey, G. K. Shukla, S. Singh, S. Sadhukhan, S. Kanungo, A. K. Jena, S. C. Lee, S. Bhattacharjee, J. Minar, and S. W. D'Souza, Role of chemical disorder in tuning the Weyl points in vanadium doped Co$_2$TiSn, Phys. Rev. Mater. **5**, 124201 (2021).

[13] B. Agrawal, A. Nagpal, R. Kumar, H. S. Saini, M. K. Kashyap, and M. Singh, *in Study of* FeCrSn$_{1-x}$Ga$_x$ *Heusler Alloys: Tuning*

Fermi Level to Attain Half-Metallic Ferromagnetism, AIP Conf. Proc. No. 2093 (AIP, Melville, NY, 2019), p. 20019.

[14] X. L. Wang, Proposal for a new class of materials: Spin gapless semiconductors, Phys. Rev. Lett. **100**, 156404 (2008).

[15] W. Q. Li, J. X. Cao, J. W. Ding, and X. H. Yan, Tuning Fermi level within half-metallic gap in Co-based Heusler alloys, Eur. Phys. J. B **85**, 250 (2012).

[16] Y. Sakuraba, K. Takanashi, Y. Kota, T. Kubota, M. Oogane, A. Sakuma, and Y. Ando, Evidence of Fermi level control in a half-metallic Heusler compound Co_2MnSi by Al-doping: Comparison of measurements with first-principles calculations, Phys. Rev. B **81**, 144422 (2010).

[17] R. Shan, H. Sukegawa, W. H. Wang, M. Kodzuka, T. Furubayashi, T. Ohkubo, S. Mitani, K. Inomata, and K. Hono, Demonstration of half-metallicity in Fermi-level-tuned Heusler alloy $Co_2FeAl_{0.5}Si_{0.5}$ at room temperature, Phys. Rev. Lett. **102**, 246601 (2009).

[18] Z. Cui, B. Wu, X. Ruan, Q. W. Zhou, Z. Y. Liu, X. Y. Fu, and Y. Feng, Enhancing the half-metallicity of equiatomic quaternary Heusler compound CoFeCrGe via atomic doping, Results Phys. **15**, 102533 (2019).

[19] R. Mahat, S. Kc, U. Karki, J. Y. Law, V. Franco, I. Galanakis, A. Gupta, and P. LeClair, Possible half-metallic behavior of $Co_{2-x}Cr_xFeGe$ Heusler alloys: Theory and experiment, Phys. Rev. B **104**, 014430 (2021).

[20] P. J. Brown, K. U. Neumann, P. J. Webster, and K. R. A. Ziebeck, The magnetization distributions in some Heusler alloys proposed as half-metallic ferromagnets, J. Phys.: Condens. Matter **12**, 1827 (2000).

[21] F. Ahmadian and A. Boochani, Half-metallic properties of the $Co_2Ti_{1-x}Fe_xGa$ Heusler alloys and $Co_2Ti_{0.5}Fe_{0.5}Ga$ (001) surface, Physica B (Amsterdam, Neth.) **406**, 2865 (2011).

[22] B. S. D. C. S. Varaprasad, A. Srinivasan, Y. K. Takahashi, M. Hayashi, A. Rajanikanth, and K. Hono, Spin polarization and Gilbert damping of $Co_2Fe(Ga_xGe_{1-x})$ Heusler alloys, Acta Mater. **60**, 6257 (2012).

[23] J. Hafner, *Ab-initio* simulations of materials using VASP: Density-functional theory and beyond, J. Comput. Chem. **29**, 2044 (2008).

[24] P. E. Blöchl, Projector augmented-wave method, Phys. Rev. B **50**, 17953 (1994).

[25] S. Kaprzyk and A. Bansil, Green's function and a generalized Lloyd formula for the density of states in disordered muffin-tin alloys, Phys. Rev. B **42**, 7358 (1990).

[26] S. Blügel, H. Akai, R. Zeller, and P. H. Dederichs, Hyperfine fields of $3d$ and $4d$ impurities in nickel, Phys. Rev. B **35**, 3271 (1987).

[27] H. Katayama, K. Terakura, and J. Kanamori, Hyperfine field of positive muon in ferromagnetic nickel, Solid State Commun. **29**, 431 (1979).

[28] N. Marzari and D. Vanderbilt, Maximally localized generalized Wannier functions for composite energy bands, Phys. Rev. B **56**, 12847 (1997).

[29] I. Souza, N. Marzari, and D. Vanderbilt, Maximally localized Wannier functions for entangled energy bands, Phys. Rev. B **65**, 035109 (2001).

[30] A. A. Mostofi, J. R. Yates, Y. S. Lee, I. Souza, D. Vanderbilt, and N. Marzari, Wannier90: A tool for obtaining maximally-localised Wannier functions, Comput. Phys. Commun. **178**, 685 (2008).

[31] N. Nagaosa, J. Sinova, S. Onoda, A. H. MacDonald, and N. P. Ong, Anomalous Hall effect, Rev. Mod. Phys. **82**, 1539 (2010).

[32] L. Bainsla, A. I. Mallick, M. M. Raja, A. A. Coelho, A. K. Nigam, D. D. Johnson, A. Alam, and K. G. Suresh, Origin of spin gapless semiconductor behavior in CoFeCrGa: Theory and experiment, Phys. Rev. B **92**, 045201 (2015).

[33] I. Galanakis, P. Mavropoulos, and P. H. Dederichs, Electronic structure and Slater–Pauling behaviour in half-metallic Heusler alloys calculated from first principles, J. Phys. D: Appl. Phys. **39**, 765 (2006).

[34] H. L. Huang, J. C. Tung, and G. Y. Guo, Anomalous Hall effect and current spin polarization in Co_2FeX Heusler compounds (X = Al, Ga, In, Si, Ge, and Sn): A systematic *ab initio* study, Phys. Rev. B **91**, 134409 (2015).

[35] S. Ouardi, G. H. Fecher, C. Felser, and J. Kübler, Realization of spin gapless semiconductors: The Heusler compound Mn_2CoAl, Phys. Rev. Lett. **110**, 100401 (2013).

[36] G. Z. Xu, E. K. Liu, Y. Du, G. J. Li, G. D. Liu, W. H. Wang, and G. H. Wu, A new spin gapless semiconductors family: Quaternary Heusler compounds, Europhys. Lett. **102**, 17007 (2013).

[37] X. B. Liu and Z. Altounian, Volume dependence of the exchange interaction and Curie temperature in Co_2MGa (M = Ti and Fe): A first-principles study, J. Appl. Phys. **109**, 07B108 (2011).

[38] H. Z. Luo, G. D. Liu, F. B. Meng, L. L. Wang, E. K. Liu, G. H. Wu, X. X. Zhu, and C. B. Jiang, Slater–Pauling behavior and half-metallicity in Heusler alloys Mn_2CuZ (Z = Ge and Sb), Comput. Mater. Sci. **50**, 3119 (2011).

[39] H. Z. Luo, F. B. Meng, H. Y. Liu, J. Q. Li, E. K. Liu, G. H. Wu, X. X. Zhu, and C. B. Jiang, Origin of the $Z-28$ rule in Mn_2Cu-based Heusler alloys: A comparing study, J. Magn. Magn. Mater. **324**, 2127 (2012).

[40] G. J. Li, E. K. Liu, Y. J. Zhang, Y. Du, H. W. Zhang, W. H. Wang, and G. H. Wu, Structure, magnetism, and magnetic compensation behavior of $Co_{50-x}Mn_{25}Ga_{25}+x$ and $Co_{50-x}Mn_{25+x}Ga_{25}$ Heusler alloys, J. Appl. Phys. **113**, 103903 (2013).

[41] D. Rani, L. Bainsla Enamullah, K. G. Suresh, and A. Alam, Spin-gapless semiconducting nature of Co-rich $Co_{1+x}Fe_{1-x}CrGa$, Phys. Rev. B **99**, 104429 (2019).

[42] D. Rani, D. K. Pandey, Y. Kimura, R. Y. Umetsu, and R. Chatterjee, Structural, magnetic, and transport properties of epitaxial thin films of equiatomic quaternary CoFeCrGa Heusler alloy, J. Appl. Phys. **132**, 193907 (2022).

[43] See Supplemental Material at http://link.aps.org/supplemental/10.1103/PhysRevB.108.224407 for the investigation of swap disorder in Cr_2FeGa; the calculated spin polarization and DOS of Cr_2FeGa with swap disorder of different degree; and the details of the carrier concentration and ordinary Hall ceffient for CoCrFeGa.

[44] M. E. Jamer, G. E. Sterbinsky, G. M. Stephen, M. C. DeCapua, G. Player, and D. Heiman, Magnetic properties of low-moment ferrimagnetic Heusler Cr_2CoGa thin films grown by molecular beam epitaxy, Appl. Phys. Lett. **109**, 182402 (2016).

[45] H. Z. Luo, L. Yang, B. H. Liu, F. B. Meng, and E. K. Liu, Atomic disorder in Heusler alloy Cr_2CoGa, Phys. B (Amsterdam, Neth.) **476**, 110 (2015).

[46] M. Zhang, E. Brück, F. R. de Boer, Z. Z. Li, and G. H. Wu, The magnetic and transport properties of the Co_2FeGa Heusler alloy, J. Phys. D: Appl. Phys. **37**, 2049 (2004).

[47] N. Kawamiya, Y. Nishino, M. Matsuo, and S. Asano, Electrical-resistance maximum near the Curie point in $(Fe_{1-x}V_x)_3Ga$ and $(Fe_{1-x}Ti_x)_3Ga$, Phys. Rev. B **44**, 12406 (1991).

[48] Y. Venkateswara, S. Gupta, S. S. Samatham, M. R. Varma, Enamullah, K. G. Suresh, and A. Alam, Competing magnetic and spin-gapless semiconducting behavior in fully compensated ferrimagnetic CrVTiAl: Theory and experiment, Phys. Rev. B **97**, 054407 (2018).

[49] M. E. Jamer, Y. J. Wang, G. M. Stephen, I. J. McDonald, A. J. Grutter, G. E. Sterbinsky, D. A. Arena, J. A. Borchers, B. J. Kirby, L. H. Lewis, B. Barbiellini, A. Bansil, and D. Heiman, Compensated ferrimagnetism in the zero-moment Heusler alloy Mn_3Al, Phys. Rev. Appl. **7**, 064036 (2017).

[50] N. F. Mott, E. A. Davis, and K. Weiser, Electronic processes in non-crystalline materials, Phys. Today **25**, 55 (1972).

[51] Y. V. Kudryavtsev, Y. P. Lee, Y. J. Yoo, M. S. Seo, J. M. Kim, J. S. Hwang, J. Dubowik, K. W. Kim, E. H. Choi, and O. Prokhnenko, Transport properties of Co_2CrAl Heusler alloy films, Eur. Phys. J. B **85**, 19 (2012).

[52] J. H. Mooij, Electrical conduction in concentrated disordered transition metal alloys, Phys. Status Solidi A **17**, 521 (1973).

[53] I. M. Tsidilkovski, Insulators, semiconductors, metals, in *Electron Spectrum of Gapless Semiconductors*, Springer Series in Solid State Sciences Vol. 116 (Springer, New York, 1997), p. 53.

[54] N. Shahi, A. K. Jena, G. K. Shukla, V. Kumar, S. Rastogi, K. K. Dubey, I. Rajput, S. Baral, A. Lakhani, S. C. Lee, S. Bhattacharjee, and S. Singh, Antisite disorder and Berry curvature driven anomalous Hall effect in the spin gapless semiconducting Mn_2CoAl Heusler compound, Phys. Rev. B **106**, 245137 (2022).

[55] Z. H. Xia, Z. H. Liu, Q. Q. Zhang, Y. J. Zhang, and X. Q. Ma, Magnetic and anomalous transport properties in spin-gapless semiconductor like quaternary Heusler alloy CoFeTiSn, J. Magn. Magn. Mater. **553**, 169283 (2022).

[56] Y. Tian, L. Ye, and X. Jin, Proper scaling of the anomalous Hall effect, Phys. Rev. Lett. **103**, 087206 (2009).

[57] K. Manna, L. Muechler, T. H. Kao, R. Stinshoff, Y. Zhang, J. Gooth, N. Kumar, G. Kreiner, K. Koepernik, R. Car, J. Kübler, G. H. Fecher, C. Shekhar, Y. Sun, and C. Felser, From colossal to zero: Controlling the anomalous Hall effect in magnetic Heusler compounds via Berry curvature design, Phys. Rev. X **8**, 041045 (2018).